Performance comparison of spectrometer based and swept source based phase sensitive optical coherence tomography

Yong Hu, George Dobre
Applied Optics Group, University of Kent, Canterbury, United Kingdom, CT2 7NH
yh95@kent.ac.uk

ABSTRACT

Spectrometer based and swept source based phase sensitive Fourier Domain OCT systems are compared in terms of the stability of the retrieved signal phase. The spectrometer based system performs with a significantly better phase stability with less uncertainty in the output, whereas the output of the swept source based system is influenced by the jitter noise that creates jumps to the retrieved phase. The experimentally obtained phase traces from the spectrometer based system match well to relevant mathematics.

Keywords: phase sensitive, spectrometer, swept source, OCT

1. INTRODUCTION

Fourier domain optical coherence tomography (FDOCT) is a noninvasive optical imaging modality capable of providing corss-sectional and 3D images of tissue structure [1]. FDOCT can be implanted in two ways: spectrometer based OCT (Sp-OCT) employing a broadband light source and a spectrometer; or swept source OCT (SS-OCT) employing a swept-laser source and a photodetector. Typically, Sp-OCT has an imaging depth less than 2 mm in air and an A-scan acquisition rate of hundreds of kHz [2], whereas SS-OCT exceeds a few centimeters imaging depth and multi MHz A-scan rate [3]. Sp-OCT performs better signal stability compared with SS-OCT [4,5]. Conventional FDOCT provides a micrometer scale resolution that is determined by the coherence gate of the system. Any refractive index change in the coherence gate or any micro vibration of the sample smaller than the coherence gate could not be detected by the conventional FDOCT. However, the detection can be deducted by a phase sensitive FDOCT system. Both Sp-OCT and SS-OCT configured systems have the phase detection function. We have built up two systems capable of retrieving phase as the signal to perform measurements on a target generating micro vibration. In this study, we compare the phase measurement performance of the Sp-OCT system and the SS-OCT system we built. Results of extra measurements from the Sp-OCT system are also presented here to check that the retrieved signal phase match to the previously proved theory.

2. THEORY

The concept of using phase sensitive Fourier Domain OCT (FD-OCT) to measure nanometre scale vibrations and displacements has been studied previously [6-10]. Assuming the detected interference term of the spectrum is $I(k) = 2|E_R E_S|cos(2kz + \varphi)$, where $k = 2\pi/\lambda$. z is the axial depth coordinate in the sample, and φ is the random system noise contributing to phase. The depth resolved magnitude $A(z)$ and phase $\Phi(z)$ information of the sample is retrieved by performing a complex Fourier transform to $I(k)$ to obtain the interference signal $I(z)$ in time domain:

$$I(z) = FT[I(k)] = A(z)exp[i\Phi(z)] \tag{1}$$

where the magnitude $A(z)$ is used to reconstruct conventional OCT images. Variation of phase $\Phi(z)$ is caused by the local optical path difference (OPD) change over time within the coherence gate at the depth z, and the phase term in Eq. (1) can be expressed as

$$\Phi(z,t) = 2 \times \frac{2\pi}{\lambda} \times n \cdot L(t) + \varphi \tag{2}$$

where $L(t)$ is the time dependent OPD value within the OCT coherence gate, n is the refractive index of the medium, and the factor 2 comes from the double path of the beam in the OCT sample arm. Assuming $L(t)$ varies in a sinusoidal manner with magnitude A and frequency f_0, Eq. (2) becomes

$$\Phi(z,t) = 2 \times \frac{2\pi}{\lambda} \times n \cdot A \cdot \sin(2\pi f_0 t) + \varphi \tag{3}$$

A differentiation operation performed on both sides of Eq. (3) results in the phase difference $\Delta\Phi(z,t)$ between successive A-scans separated by an time interval Δt,

$$\Delta\Phi(z,t) = \frac{8\pi^2}{\lambda} \times n \cdot A \cdot f_0 \cdot \cos(2\pi f_0 t) \cdot \Delta t \tag{4}$$

Thus, with the depth z fixed, either by measuring $\Phi(z,t)$ in Eq. (3), or by measuring $\frac{\Delta\Phi(z,t)}{\Delta t}$ in Eq. (4), the local vibration amplitude A of the sample can be calculated. In this study, Eq. (2, 3, 4) are being used to test the performance of phase sensitive Sp-OCT and SS-OCT systems.

3. EXPERIMENT

3.1 System configuration

The structure of the phase sensitive Spectrometer-based (Sp-OCT) system is illustrated in Fig. 1. The OCT source is a superluminescent diode (Amonics, ALS-1050-S) with an output power of 13 mW and a spectral full-width at half maximum (FWHM) of 35 nm centered at 1050 nm, resulting in a theoretical axial resolution of 14 µm in air. The output light enters a fiber isolator (AFW Technologies, ISOD-64) and subsequently a 2×2 fiber-optic Michelson interferometer through a 50:50 fiber coupler (THORLABS, TW1064R5A2A), with 50% going to the reference arm and 50% to the sample arm. Both fiber outputs of the coupler are pigtailed to collimators (THORLABS, F260APC-1064) creating a beam size of 2.4 mm in free space. In the sample arm, the beam hits two galvanometer mirrors (THORLABS, GVS302) and subsequently an objective / scan lens (THORLABS, LSM02-BB, f =110 mm) producing a focused spot size of 28 µm on the target. In the reference arm, a glass dispersion compensation block (THORLABS, LSM02DC) compensates the dispersion created by the double paths of the objective lens in the sample arm. Light returning from two arms are recombined and delivered to a spectrometer consisting a high speed line scan CCD camera (GOODRICH SUI, SU1024-LDH) with the maximum line rate of 47000 kHz and the digital output rate of 14-bit. The CCD has 1024 elements with pixel size of 25 µm × 500 µm and a spectral range of 900 nm, resulting in the spectral resolution $\delta\lambda$ = 0.88 nm at the center wavelength λ_0 = 1050 nm. The detected interference signal is digitized by a camera link image acquisition card (NATIONAL INSTRUMENTS, PCIe-1430) installed in a computer to generate a spectrum with points attributed non-linear in k-space. In Sp-OCT, it is crucial to rescale and resample the spectral data to make them evenly attribute in k-space. The resampling algorithm employed here is the B-spline interpolation (carried out in Labview post-processing). After the resampling, the interference pattern of each A-scan is complex Fourier transformed to retrieve the depth-resolved intensity $A(z)$ and phase $\Phi(z)$ profile of the detected sample.

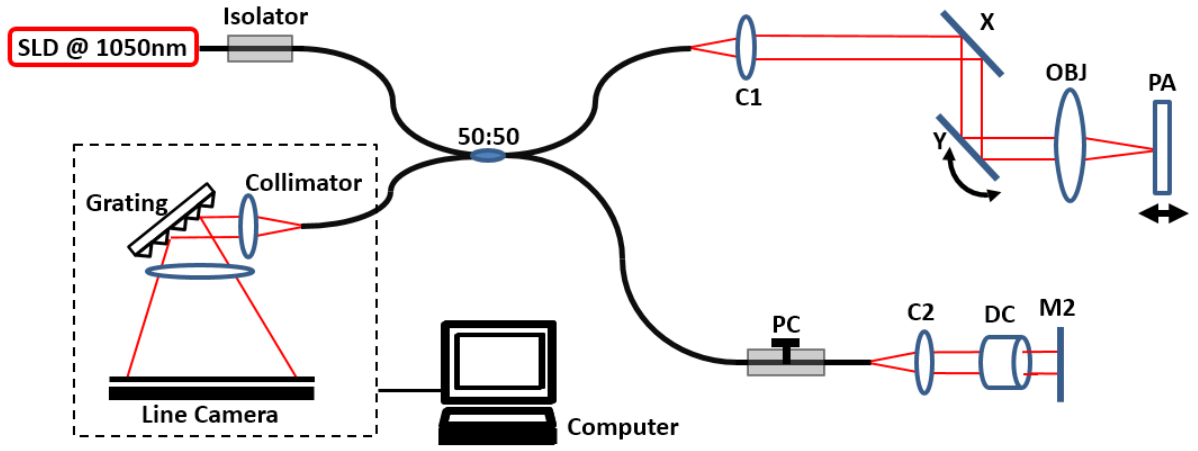

Fig. 1. Schematic of phase sensitive Sp-OCT system. Superluminescent diode light source (SLD); 2 by 2 fiber splitter (50:50); Collimating lenses (C1, C2). Stationary mirrors (M2); Objective/scan lens (OBJ); Galvanometer mirrors (X, Y); Dispersion compensating block (DC); Piezoelectric actuator (PA).

The phase sensitive Swept Source (SS-OCT) system schematic is illustrated in Fig. 2. The swept source (AXSUN Technology, 1060) has a central wavelength of 1060 nm, a FWHM bandwidth of 100 nm, a duty cycle of 46%, and a sweep rate of 100 kHz. The SS-OCT system has a measured axial resolution δz of 10 µm (FWHM amplitude profile) which remains constant throughout the 3.5 mm imaging range in air. The interferometer is constructed by a fiber array. 20% of the light proceeds to the sample arm, and 80% to the reference arm. In the object arm, the propagation is identical to the Sp-OCT case. In the reference arm, two dispersion compensation blocks are used. The light returning from the reference mirrors and 80% of the light reflected by the sample interfere at the output of a 50:50 coupler. The interference signal is detected by a balanced photodetector (THORLABS, PDB430C, DC to 350 MHz bandwidth) which also removes the DC component in the signal. The digitized interference signal is subsequently acquired by a 12 bit waveform digitizer (AlazarTech, ATS9350, sampling rate 500 MS/s). The input trigger on the digitizer is connected with the output trigger on the swept laser that generates a trigger at the beginning of each sweep to trigger the data acquisition process of the digitizer [4].

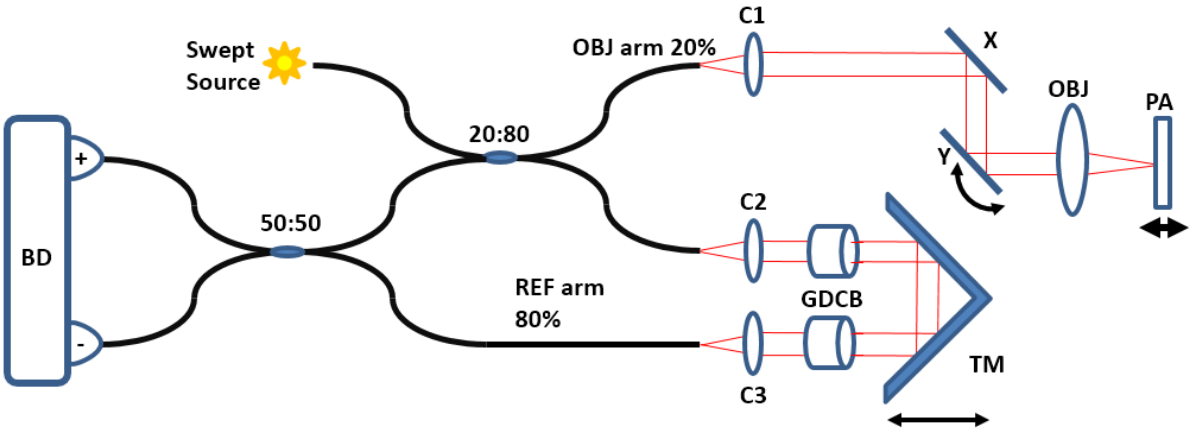

Fig. 2. Schematic of phase sensitive SS-OCT system. 2 by 2 fiber splitter (50:50, 20:80); Collimating lenses (C1, C2, C3); Translation mirrors (TM); Objective/scan lens (OBJ); Galvanometer mirrors (X,Y); Dispersion compensating blocks (GDCB); Piezoelectric actuator (PA); Balanced photodetector (BD).

The digitizer uses an external clock obtained from the output clock on the swept laser. The swept laser generates a clock uniform in k-space, which enables the digitizer to perform uniform data sampling in k-space. Thus, in SS-OCT, no data resampling or processing is required. Connecting the trigger and the clock in this way allows direct k-clock sampling to take place, which overcomes the nonlinear spectral sweeps.

3.2 Sample preparation and phase retrieval

As demonstrated in Fig. 3, the vibrating sample used in the study is a piezo-mounted (THORLABS, PA4FEW) microscope coverslip (100 µm thick). The signal phase was measured on the front surface of this coverslip. Since the data along the axial direction were acquired at the same time in each A-scan, they shared a common mode noise that was due to the mechanical or thermal fluctuations in each independent arm [6,10]. To remove this common mode noise, a stationary coverslip was placed in front of the actuated coverslip to provide a reference phase. Assuming the mechanical or thermal fluctuations between two coverslips can be ignored, the noise contributed by the fluctuations outside can be removed by subtracting the reference phase from the signal phase. Thereby, the motion of the actuated coverslip was the only factor contributing to the variation of the difference between the signal phase and the reference phase. In the study, the phase difference is used as the phase signal.

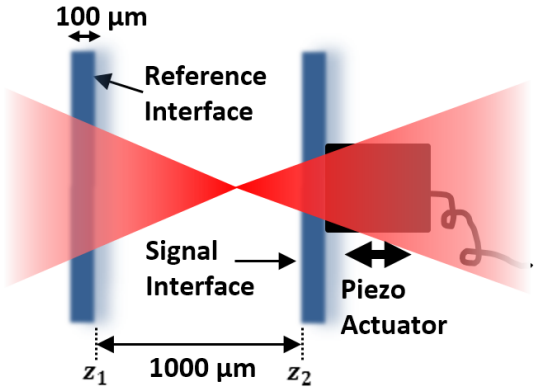

Fig. 3. Vibrating sample: piezo-mounted 100 µm microscope coverslip. Signal phase is measured on the signal interface at z_2; The reference interface at z_1 provides the reference phase to remove the common mode noise. The beam focus is located between two coverslips.

In both Sp-OCT and SS-OCT systems, the phase signal was retrieved by following procedures: first, 1024 samples were recorded to generate a digitized A-scan interference spectrum. Two LabVIEW programs, both with an A-scan acquisition rate of 500 Hz, were designed for corresponding systems. The LabVIEW program for the Sp-OCT system had the resampling algorithm performing on the interference spectrum, whereas this function is omitted in the SS-OCT system. Then, the interference pattern was complex Fourier transformed to produce a 512-pixel A-scan intensity profile as a function of depth showing axial features of the sample. From this intensity pattern, the pixel orders corresponding to the reference interface at z_1 (Fig. 3) and the investigated interface or axial position were identified and selected. In each single A-scan, the LabVIEW program retrieve and unwrap phase values of these two selected pixels. Last, the difference between these retrieved phase values was calculated to be used as the phase signal in the study.

4. RESULTS

4.1 Side by side comparison of signal outputs from Sp-OCT and SS-OCT systems

The system noise determines the minimum detectable phase variation of an OCT system. To study and compare the minimum detectable phases of the Sp-OCT system and the SS-OCT system, the reference pixel and the investigated pixel were chosen in the same coherence gate. The A-scan peak of the reference inter phase (Fig. 3) is composed of 5 pixels in the amplitude A-scan profile. Within the peak, phase values were retrieved from two adjacent pixels most closed to the highest point. The difference of these phase values were calculated as the signal phase $\Phi(z_2,t)$ for plotting traces in Fig. 4 (A) and (B).

Ideally, if no system noises present in a OCT system, $\Phi(z_2,t)$ should be always 0 rad as no relative motion existing between two adjacent pixels in a coherence gate. Thus, the fluctuations of $\Phi(z_2,t)$ traces around 0 rad in Fig. 4 (A) and (B) reflect different noise levels for the two systems. Comparing the level of random fluctuations on traces in Fig. 4 (A) and (B), the uncertainty of signal phase $\Phi(z_2,t)$ in Sp-OCT system is significantly better than that of the SS-OCT system. The noticeable step in Fig. 4 (B) happened very often during the measurement. It came from the jitter noise of the swept source employed in the SS-OCT system, which was generated by the uncertain relative phase relationship between successive spectrum sweep of the source.

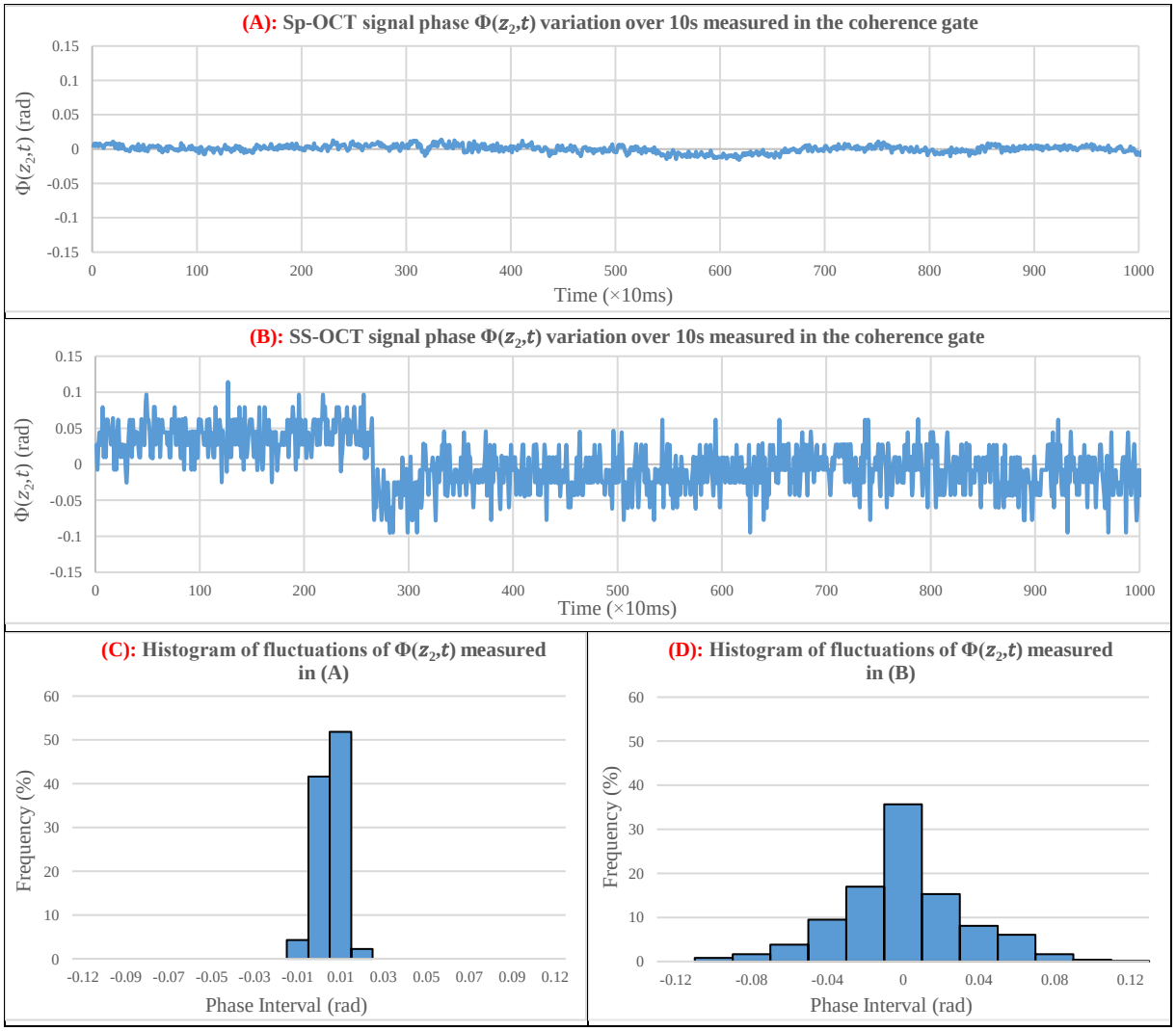

Fig. 4. Dynamic output signal phase $\Phi(z_2,t)$ measured in the coherence gate of (A): Sp-OCT system and (B): SS-OCT system. (C): histogram of $\Phi(z_2,t)$ values in (A). (D): histogram of $\Phi(z_2,t)$ values in (B).

To analyze and quantify the noise level difference of the two systems, the $\Phi(z_2,t)$ values in Fig. 4 (A) and (B) are grouped to histograms shown in Fig. (C) and (D). Comparing Gaussian fits of Fig. (C) and (D), the full width at half maximum (FWHM) of two graphs indicates that the signal phase uncertainty of Sp-OCT system is 4 times better than that of the SS-OCT system.

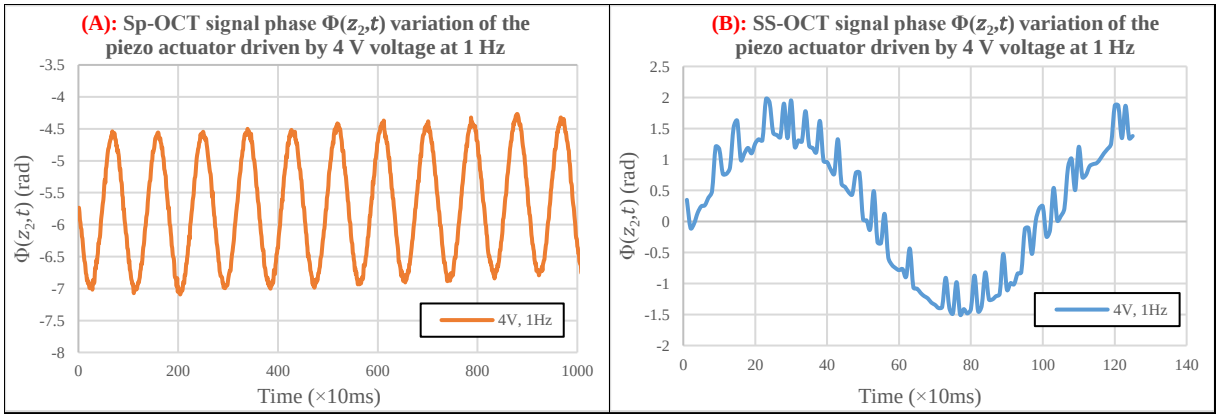

Fig. 5. Dynamic output signal phase $\Phi(z_2,t)$ measured on the surface of an actuated coverslip form (A): Sp-OCT system and (B): SS-OCT system. The piezo actuator is driven by a sinusoidal voltage with the frequency of 1 Hz and amplitudes of 4 V.

Extra measurements were taken on the front surface of the piezo actuator-mounted coverslip (Fig. 3) for both systems. The actuator was driven a sinusoidal voltage with the frequency of 1 Hz and amplitudes of 4 V. As can be seen in Fig. 5 (A) and (B), the signal phase $\Phi(z_2,t)$ measured from both systems present sinusoidal appearance with expected frequency. The $\Phi(z_2,t)$ trace from the Sp-OCT system is clean, whereas the $\Phi(z_2,t)$ trace from the SS-OCT system is added with spikes which disturb the reading of the amplitude. Even though the spikes could have been removed by filtering treatments, the existence of them indicates a more noisy nature of the SS-OCT system compared with the Sp-OCT system.

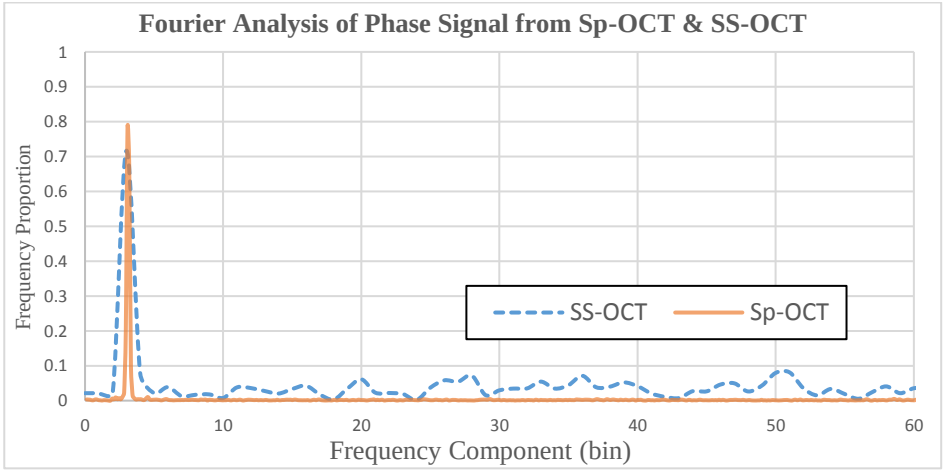

Fig. 6. Fourier analysis performed on 120 data points on traces of Fig. 5. (A) Orange line: Fourier analysis of Sp-OCT output. Dotted line: Fourier transform of Fig. 5 (B) obtained from the SS-OCT. The peak widths are in a ratio of 8.5:1.

To analyze the spectrum components of two $\Phi(z_2,t)$ traces in Fig. 5 (A) and (B), a Fourier transform was performed on continuous 120 data points in both Fig. 5 (A) and (B). As can be seen from Fig. 6, the frequency components of the $\Phi(z_2,t)$ trace from the Sp-OCT (orange trace) is purer than that from the SS-OCT (blue trace). As shown by the orange trace, 80% of the frequency components are concentrated around the driving frequency of the vibrating target for the Sp-OCT. The higher frequency components in the blue trace agree with the spikes on the $\Phi(z_2,t)$ trace in Fig. 5 (B).

4.2 Phase sensitive Sp-OCT – further aspects

The results in section 4.1 indicate that the Sp-OCT system performs with a significantly better signal phase stability than that of the SS-OCT system. In order to further investigate the performance of the Sp-OCT system, a series of measurements were performed on the vibrating target to check if the experimentally obtained $\Phi(z_2,t)$ and $\Delta\Phi(z_2,t)$ traces match to Eq. (3) and Eq. (4).

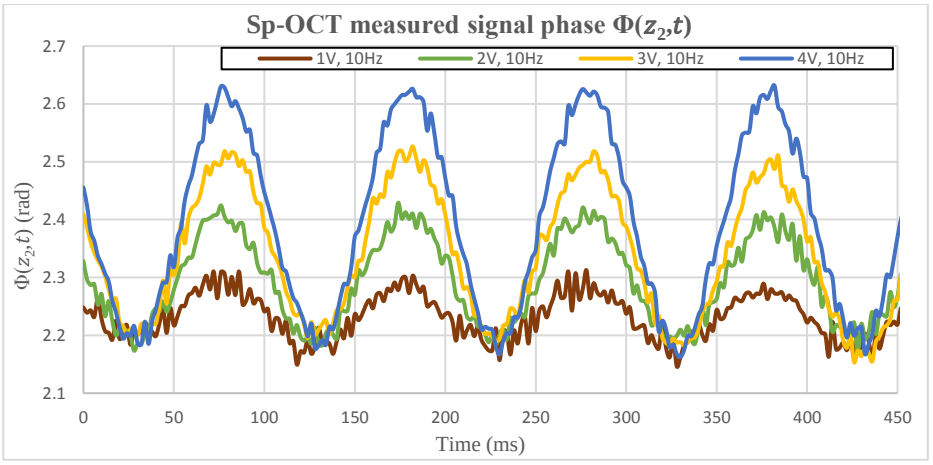

Fig. 4. Sp-OCT measured signal phase $\Phi(z_2,t)$. The piezo actuator was driven by sinusoidal voltages with fixed frequency (10Hz) and different amplitudes (1V, 2V, 3V, 4V).

The piezo actuator was firstly driven by sinusoidal voltages first with a fixed frequency (10Hz) and different amplitudes (1V, 2V, 3V, 4V), then with a fixed amplitude (4V) and different frequencies (5Hz, 10Hz, 15Hz, 20Hz). The measured dynamic $\Phi(z_2,t)$ traces of two groups of driving parameters are presented in Fig. 4 and Fig. 5 respectively. During the measurement, a random phase drift (presented as φ in Eq. (3)) added a varying DC component to $\Phi(z_2,t)$. For ease of comparison, $\Phi(z_2,t)$ traces are overlapped in Fig. 4 and Fig. 5.

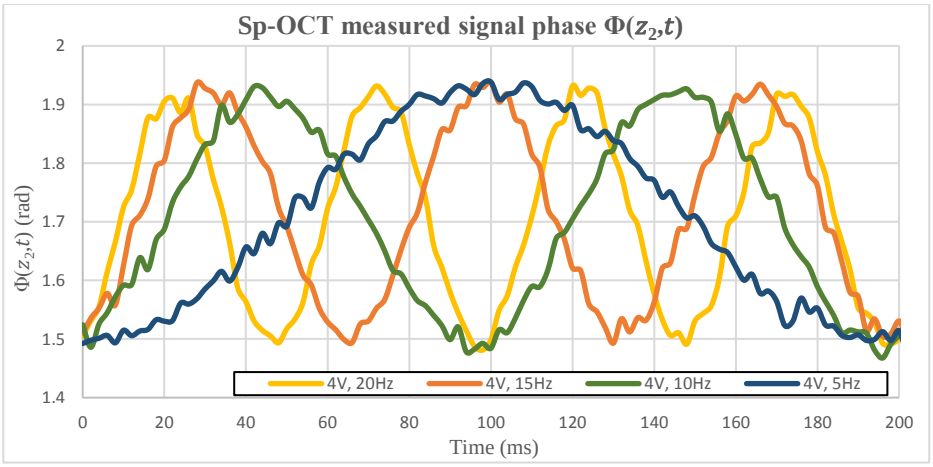

Fig. 5. Sp-OCT measured signal phase $\Phi(z_2,t)$. The piezo actuator was driven by sinusoidal voltages with fixed amplitude (4V) and different frequencies (5Hz, 10Hz, 15Hz, 20Hz).

As seen in Fig. 4, the measured $\Phi(z_2,t)$ traces have the same modulation frequency that equals to the sinusoidal frequency of the detected movement. As expected, the amplitudes of these traces are different as the driving voltages of the actuator are different. As seen in Fig. 5, the measured $\Phi(z_2,t)$ traces have the same amplitude but different modulation frequencies equivalent to the corresponding to the vibrating frequencies of the target. All measured $\Phi(z_2,t)$ traces in Fig. 4 and Fig. 5 agree with Eq.(3) where the modulation frequency of $\Phi(z_2,t)$ varies with the vibrating frequency f_0, and the modulation amplitude of $\Phi(z_2,t)$ varies with the vibrating amplitude A of the actuator. During the measurement, the random phase drift was added on the dynamic $\Phi(z_2,t)$ trace very often. The drift caused the signal to move in an unwanted fashion, which created inconvenience and prompted us to generate the phase differential $\Delta\Phi(z_2,t)$ trace, as discussed below.

To generate dynamic $\Delta\Phi(z_2,t)$ traces and check if they match to Eq.(4), another LabVIEW program was designed to calculate the difference between signal phases $\Delta\Phi(z_2,t+\Delta t)$ and $\Phi(z_2,t)$, which were obtained from successive A-scans with a time interval of Δt = 2 ms (500 Hz A-scan rate). The actuator was driven by sinusoidal voltages first with a fixed amplitude (4V) and different frequencies (10Hz, 25Hz), then with a fixed frequency (5Hz) and different amplitudes (14V, 28V, 42.5V). Results are presented in Fig. 6 and Fig. 7 respectively.

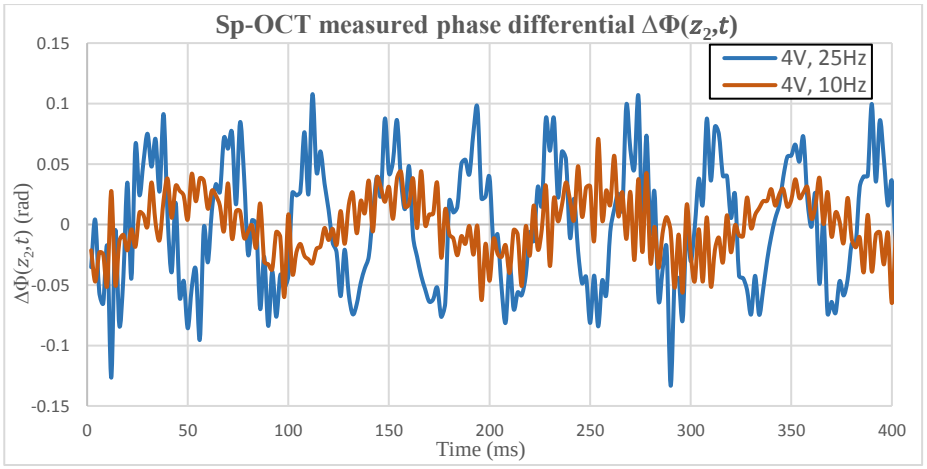

Fig. 6. Sp-OCT measured phase differential $\Delta\Phi(z_2,t)$. The piezo actuator was driven by sinusoidal voltages with fixed voltage (4V) and different frequencies (10Hz, 25Hz).

As seen in Fig. 6, unlike the traces in Fig. 5, the amplitudes of $\Delta\Phi(z_2,t)$ traces vary with the vibrating frequency of the actuator. This agrees with Eq.(4), where the vibrating frequency f_0 is a factor multiplying the cosine term and modifies the amplitude of $\Delta\Phi(z_2,t)$. As seen in Fig. 7, with the vibrating frequency of the actuator fixed but the vibrating amplitude changed, the modulation frequencies of $\Delta\Phi(z_2,t)$ traces are equal to the vibrating frequency of the actuator and the amplitudes of $\Delta\Phi(z_2,t)$ traces are different. Again this agrees with Eq. (4), where the vibrating amplitude A is a factor of the modulation amplitude of $\Delta\Phi(z_2,t)$ and has no impact on the modulation frequency of $\Delta\Phi(z_2,t)$. As seen from both graphs, unlike the case of $\Phi(z_2,t)$ traces, the $\Delta\Phi(z_2,t+\Delta t)$ traces vary about 0 rad with no DC drift added. This is because the differentiation operation on $\Phi(z_2,t)$ eliminates φ in Eq. (3).

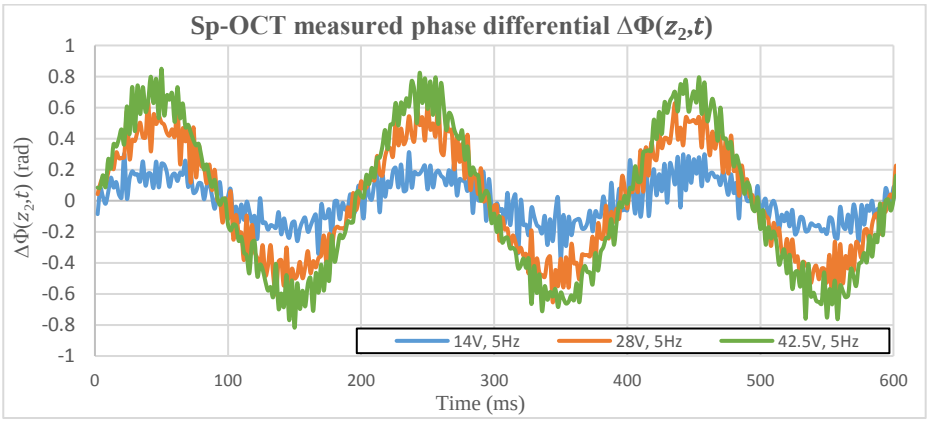

Fig. 7. Sp-OCT measured phase differential $\Delta\Phi(z_2,t)$. The piezo actuator was driven by sinusoidal voltages with fixed frequency (5Hz) and different amplitudes (14V, 28V, 42.5V).

We sent sinusoidal voltages with different amplitudes (2 V, 3 V, 4 V) and frequencies (1 Hz to 20 Hz with 1 Hz interval) to the actuator, and then used Eq. (4) to convert the amplitudes of $\Delta\Phi(z_2,t)$ into the displacement amplitude A. Results are presented in Fig. 8. As can be seen, from 1 Hz to 20 Hz, the vibrating amplitude of the actuator is more determined by the amplitude of the driving voltage and has less dependence on the driving frequency. This is an expected result, as the actuator is supposed to have a sustaining displacement to voltage amplitude performance at low driving frequencies.

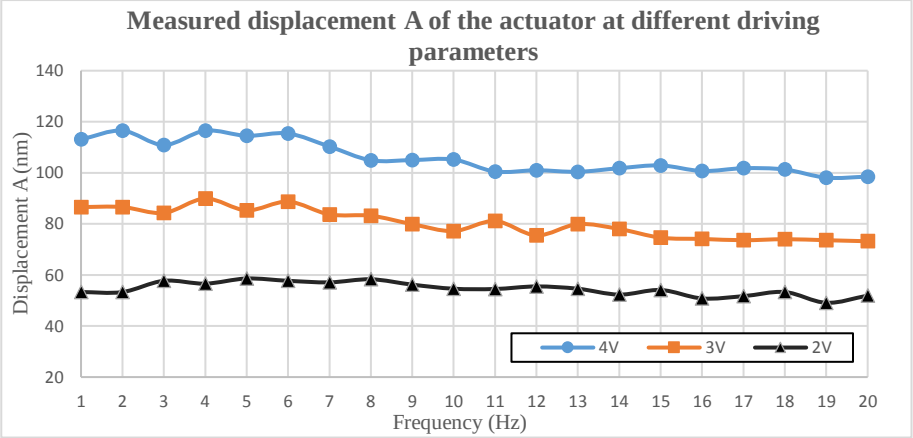

Fig. 8. Measurement of the displacement A of the actuator at different driving parameters. The actuator is driven by sinusoidal voltages with different amplitudes (2 V, 3 V, 4 V) and frequencies (1 Hz to 20 Hz with 1 Hz interval).

5. CONCLUSIONS

We performed a direct comparison of the output stability performance of a spectrometer based OCT system and swept source based OCT system, both using the identical object arm (including sample) and the same data acquisition speed. To eliminate the moving air induced influence, we employed a reference interface to provide a reference phase. The signal phase used in the study was the difference between the measured phase at an interested location and the reference phase. It is found that the stability of the retrieved signal phase is clearly superior for the Sp-OCT system. The uncertainty caused by the system noise in the Sp-OCT was found to be 4 times smaller than that of the SS-OCT. Moreover, the Sp-OCT exhibits no phase jump in the signal phase output. Compared with it, the SS-OCT is affected by the jitter noise in the swept source which causes random jumps in the output.

Since the proved advantage of signal stability of the Sp-OCT system, we performed a series of measurement for a further investigation of its performance. All experimentally obtained signal phase traces measured by the Sp-OCT behave in expected ways. The modulation frequencies and amplitudes of these traces match to the previously proved theory with mathematics. Employing these math equations, we have converted measured phase to absolute vibrating amplitudes.

REFERENCES

[1] A. Gh. Podoleanu, “Optical Coherence Tomography,” Journal of Microscopy 247(3), 209-299 (2012).

[2] Y. Zhang, B. Cense, J. Rha, R. S. Jonnal, W. Gao, R. J. Zawadzki, J .S. Werner, S. Jones, S. Olivier, and D. T. Miller, “High-speed volumetric imaging of cone photoreceptors with adaptive optics spectral-domain optical coherence tomography,” Opt. Express 14(10), 4380-4394 (2006).

[3] R. Huber, D. C. Adler, and J. G. Fujimoto, “Buffered Fourier domain mode locking: unidirectional swept laser sources for optical coherence tomography imaging at 370,000 lines⁄s370,000 lines/s,” Opt. Lett. 31(20), 2975-2977 (2006).

[4] M. A. Choma, A. K. Ellerbee,S. Yazdanfar, and J. A. Izatt, “Doppler flow imaging of cytoplasmic streaming using spectral domain phase microscopy,” J. Biomed. Opt. 11(2), 024014 (2006).

[5] M. V. Sarunic, S. Weinberg, and J. A. Izatt, “Full-field swept-source phase microscopy,” Opt. Lett. 31(10), 1462-1464 (2006).

[6] R. Huber, D. C. Adler, J. G. Fujimoto, "Buffered Fourier Domain Mode Locking (FDML): Unidirectional swept laser sources for OCT imaging at 370000 lines per second", Optics Letters 31(20), 927-929 (2006).

[7] D. C. Adler, R. Huber, and J. G. Fujimoto, “Phase sensitive optical coherence tomography at up to 370,000 lines per second using buffered Fourier domain mode-locked lasers,” Opt. Letters 32(6), 626-628 (2007).

[8] D. C. Adler, Sh. W. Huang, R. Huber, and J. G. Fujimoto, “Photothermal detection of gold nanoparticles using phase-sensitive optical coherence tomography,” Opt. Express 16(7), 4376-4393 (2008).

[9] R. K. Wang, and A. L. Nuttall, “Phase sensitive optical coherence tomography imaging of the tissue motion within the organ of Corti at a subnanometer scale a preliminary study,” J. Biomed Opt. 15(5), 056005 (2010).

[10] Z. Chen, T. E. Milner, D. Dave, and J. S. Nelson, “Optical Doppler tomographic imaging of fluid flow velocity in highly scattering media,” Opt. Lett. 22(1), 64-66 (1997).